Journal of Materials Chemistry C

Accepted Manuscript

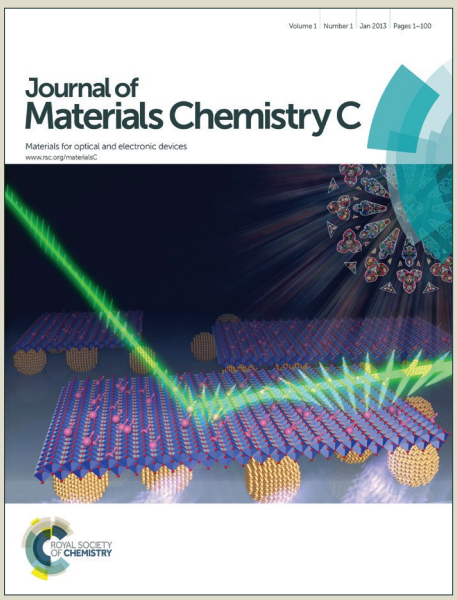

ROYAL SOCIETY OF CHEMISTRY

www.rsc.org/materialsC

Journal Name

ARTICLE

Sterically hindered diarylethenes with a benzobis(thiadiazole) bridge: photochemical and kinetic studies†

Received 00th January 20xx,
Accepted 00th January 20xx

DOI: 10.1039/x0xx00000x

www.rsc.org/

Wenlong Li,[a] Yunsong Cai,[a] Xin Li,*[b] Hans Ågren,[b] He Tian[a] and Wei-Hong Zhu*[a]

Four rationally designed diarylethenes (DAEs) **1**-**4** with a benzobis(thiadiazole) bridge are specifically designed for taking insight into steric effects on photochromic performances. It is shown that, upon increasing steric hindrance, the exchanging rate between two main conformers in the ring-open form gradually slows down, offering the opportunity to isolate the photoactive *anti*-parallel conformer. Impressively, the separated *anti*-parallel conformer show high cyclization quantum yields over the unresolved common DAEs. The typical donor-π-acceptor (D-π-A) feature in the ring-open DAEs **1**-**4** endows their prominent fluorescence, which can be conveniently modulated by photocyclization. In the ring-closed form, the excess steric hindrance is found to seriously disrupt the thermal bistability, and particularly **3c** fades quickly with a half-life of several hours at ambient temperature. In contrast, both **1c** and **2c** exhibit excellent stability, which originates from the stabilization effects of intramolecular hydrogen bonds. This work demonstrates the steric effects on the photochemical and kinetic behaviors of DAEs, providing a unique approach to develop photochromic DAEs with high photosensitivity.

1 Introduction

Photochromic derivatives have attracted much attention in that their chemical and physical properties can be readily altered by external photo-irradiation, especially for practical applications such as molecular switches,[1-7] smart materials,[8-14] and information storage.[15-19] Among various photochromic systems, diarylethenes (DAEs)[20-22] are one of the most famous organic representatives due to their outstanding thermal irreversibility and fatigue resistance. Many efforts have been focused on the structural improvements to improve photochromic performances. For instances, the first generation (I) of thermally irreversible DAEs (Scheme 1a) adopts the electron-withdrawing dicyanoethene-bridge for successfully separating the absorption bands of the ring-open (*o*-) and ring-closed (*c*-) isomers, but it unfortunately suffers from the undesirable *cis*- to *trans*- isomerization.[23] Although the second generation (II) prevents the side reaction by employing the cyclizated maleic anhydride or imide derivatives as the ethene bridge, its photochromism is often largely suppressed in polar solvents.[24] Those problems are perfectly solved in the third generation (III)[20] utilizing the perfluoro-cyclopentene bridge,[25] which is the most widely accepted framework nowadays. However, its structural extensions are strictly limited to the aryl parts, due to considerable difficulties in the modification of cycloalkene moiety.[26-28] In fact, the exploitation of ethene bridges would bring forth extra chemical and physical properties to the DAE family.[29-34] Moreover, since the ethene bridge is located closer to the photochromic center, the control of properties by introducing functional ethene bridges can sometimes be more effective than the modifications of the side aryl groups.

As a special aspect, several previous works have proved that some ethene bridges can remarkably enhance the photo-sensitivity of the cyclization reaction. Structurally, the open form *o*-DAEs possess two main exchangeable conformers with parallel (*p*-) and *anti*-parallel (*ap*-) orientations in the two aryl groups, of which only the *ap*-conformer satisfies the Woodward-Hoffmann rules, and is able to offer the corresponding closed form (*c*-DAEs) under UV irradiation (Scheme 1b).[20] Thus, increasing the ratio of the photo-active *ap*-conformer is a general method to develop new DAE systems with high photocyclization quantum yields ($\Phi_{o\text{-}c}$). Typically, Yokoyama and Kawai *et al*. utilized intramolecular weak interactions between the ethene bridge and side aryl groups to enrich the ground-state energetically-favored *ap*-conformers,[35-38] and thus achieved extremely high $\Phi_{o\text{-}c}$, even up to almost 100%. In a more direct way, Takeshita and Feringa *et al*. employed the covalent bonding and steric hindrance in the ethene bridge and aryls to obtain unmixed *ap*-conformers[39-42] that enhance the photo-switching performance. However, in order to stabilize the *ap*-

[a] *Shanghai Key Laboratory of Functional Materials Chemistry, Key Laboratory for Advanced Materials and Institute of Fine Chemicals, East China University of Science and Technology, Collaborative Innovation Center for Coal Based Energy (i-CCE), Shanghai 200237, P. R. China. Fax: (+86) 21-6425-2758. E-mail: whzhu@ecust.edu.cn.*
[b] *Division of Theoretical Chemistry and Biology, School of Biotechnology, KTH Royal Institute of Technology, SE-10691 Stockholm, Sweden. E-mail: lixin@theochem.kth.se*

† Electronic Supplementary Information (ESI) available: Supplemental data of DAEs **1**-**4** and compound characterizations, including crystal data. See DOI: 10.1039/x0xx00000x

conformers, those approaches often seriously depend on the specific conditions, and in some cases they have to sacrifice the basic virtues of DAEs such as the thermal irreversibility of coloured isomers. How to balance these extra and original properties is still a main task for practical applications.

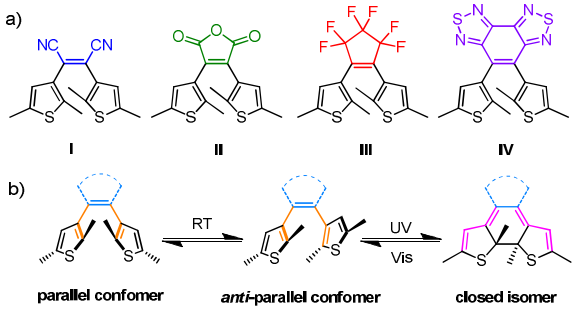

Scheme 1 a) Roadmap to develop thermally irreversible DAEs based on the modification of ethene bridge from dicyanoethene-bridge (I), maleic anhydride bridge (II), perfluoro-cyclopentene bridge (III), and sterically hindered diarylethenes with a benzobis(thiadiazole) bridge (IV). b) Ring-open and ring-closed isomers of DAEs and their interconversion.

We have reported that benzobisthiadiazole (BBT) can act as a six-membered ethene bridge to build up a unique photochromic system (DAE IV, Scheme 1a) with excellent thermal bistability.[43,44] Interestingly, the extended planar nature of the BBT bridge may generate notable steric hindrances with the adjacent benzothiophene groups, which eventually leads to thermal isolation of the pure *ap*-conformer (DAE **2a**) with high $\Phi_{o\text{-}c}$.[45,46] In order to further understand the mechanism and extend the scope of applicability, we herein report the synthesis and photochromic properties of a series of sterically hindered DAEs (**1**-**4**, Fig. 1a) based on the BBT bridge. Both experimental and theoretical results confirmed that the isomerism between the *ap*- and *p*-conformers depends on the steric sizes of side aryl groups, and only the *β*-substituted thiophene derivatives (DAEs **2** and **3**) can effectively block the spontaneous interconversion, ensuring high $\Phi_{o\text{-}c}$ of over 50%. Despite of excess hindrance, the *c*-isomers of DAEs **1** and **2** still exhibit considerable thermal irreversibility, owing to the stabilization effects from the intramolecular hydrogen bonds between the BBT bridge and side aryls. Considering all the aspects, DAE **2** is the most balanced representative with excellent stability in its *ap*- and *p*-conformers, and *c*-isomers, which is expected to serve as a promising building block for highly photo-sensitive photochromic DAE systems. Meanwhile, since steric effects have been scarcely studied in detail so far, this work can also serve as a unique platform for systematic explorations of steric effects on the isomerism and photochromism of DAEs.

2 Experimental

2.1 Materials and instruments. ^{1}H NMR and ^{13}C NMR spectra were recorded using Bruker AM-400 spectrometers with tetramethylsilane (TMS) as an internal reference. $CDCl_3$ and THF-d_8 were used as solvents. HRMS spectra were recorded using a Waters LCT Premier XE spectrometer with methanol or acetonitrile as solvents. HPLC analyses were performed by using an Agilent 1100 instrument equipped with C18 column (250 × 4.6 mm, Agilent Technologies). Absorption and fluorescence spectra were recorded using Varian Cary 500 and HORIBA Fluoromax 4 instruments, respectively. The photochromic reaction was induced *in situ* by continuous irradiation using an Hg/Xe lamp (Hamamatsu, LC8 Lightningcure, 200 W) equipped with a narrow band interference filter (Shenyang HB optical Technology) for λ_{irr} = 313 nm, a broad band interference filters (Shenyang HB optical Technology) for λ_{irr} > 470 nm, or a monochromator (Monoscan 2000, OceanOptics) for λ_{irr} = 517 nm. The photochromic reaction quantum yields were evaluated by the standard procedures using 1,2-bis(2-methylbenzo[*b*]thiophen-3-yl)perfluoro- cyclopentene as the references for photocyclization and cycloreversion. The rates of isomerization in the initial stage of the reaction (0-5%) were compared with references whose $\Phi_{o\text{-}c}$ (35%) and $\Phi_{c\text{-}o}$ (35%) in hexane are known, which brought forth 5% uncertainties on the calculations of quantum yields. The fluorescence quantum yields (Φ_F) were measured using anthracene in EtOH (27%). *o*-DAEs **2** and **4** were prepared, according to our previous work.[43,45] Solvents used were analytical grade, except those for recrystallization and optical tests, which were purified by distillation.

2.2 Synthesis

Synthesis of *o*-DAE 1 (mixer of 1a and 1p). To a fire dried three necked bottle was added 3-bromo-2-methylbenzofuran (10.00 g, 47.38 mmol) and 100 mL dried THF. The mixture was cooled to 195 K and 2.4 M BuLi (21.8 mL, 52.32 mmol) was introduced dropwise. After 1 h, trimethyl borate (8.0 mL, 70.44 mmol) was introduced. The resulting mixture was kept at 195 K for another 2 h. Then the mixture was warmed to room temperature to stay overnight. After reaction, the solvent was removed under vacuum and crude product was used directly without further treatment. The obtained oil was dissolved in dioxane (150 mL), to which 4,5-dibromobenzo[1,2-*c*:3,4-*c*']bis[1,2,5]thiadiazole (1.00 g, 2.84 mmol), $[Pd(PPh_3)_4]$ (0.70 g, 0.61 mmol), and aqueous K_2CO_3 (75 mL, 2.5 mol L^{-1}) were added. The resulting mixture was allowed to reflux under Ar in the dark for 20 h, cooled to room temperature, poured into water, and extracted with dichloromethane. The organic layer was separated and dried with anhydrous Na_2SO_4. After concentration, the residual was purified by flash column chromatography (silica, petroleum ether:dichloromethane = 4:1 v/v) to give DAE **1** (mixer of **1a** and **1p**, 0.23 g, 17.8%): slight yellow solids. ^{1}H NMR (400 MHz, $CDCl_3$, ppm): δ 1.91 (s, 3H), 2.23 (s, 3H), 6.88-6.98 (m, 2H), 7.10-7.21 (m, 3H), 7.21-7.30 (m, 1H, overlapping with $CHCl_3$), 7.31-7.38 (m, 1H), 7.40-7.46 (m, 1H). ^{13}C NMR (100 MHz, $CDCl_3$, ppm): δ 13.66, 13.96, 110.89, 111.13, 111.47, 111.89, 119.63, 119.77, 122.54, 122.78, 123.76, 123.85, 127.77, 127.92, 128.14, 128.54, 147.67, 153.89, 153.94, 153.99, 154.43, 156.75, 156.82. HRMS (ESI positive ion mode for $[M + H]^+$): Calcd for $C_{24}H_{15}N_4O_2S_2$, 455.0636; found: 455.0630.

Synthesis of 1c. *o*-DAE **1** (mixer of **1a** and **1p** 1.00 g, 2.20 mmol) was dissolved in THF (200 mL), and then irradiated with UV light (λ = 313 nm) for 3 h. After concentration, the residual was purified by column chromatography (silica, petroleum ether:dichloromethane = 4:1 v/v) to give **1c** (0.21 g, 21.0%): red needles. ^{1}H NMR (400 MHz, $CDCl_3$, ppm): δ 1.69 (s, 3H), 7.01-7.15 (m, 4H), 7.38-7.48 (m, 2H), 9.05-9.20 (m, 2H). ^{13}C NMR (100 MHz, $CDCl_3$, ppm): δ 16.43, 91.94, 111.79, 116.09, 121.39, 122.27, 129.13, 133.85, 146.65, 149.97, 156.25, 166.04. HRMS (ESI positive ion mode for $[M + H]^+$): Calcd for $C_{24}H_{15}N_4O_2S_2$, 455.0636; found: 455.0633.

Synthesis of 1a. Due to the slow exchanging between **1a** and **1p**, it is difficult to obtain pure **1a** and **1p**. Thus, **1a** was generated *in situ* from **1c** upon strong visible light (λ > 470 nm) within several minutes, either in the cuvette for optical tests or in the NMR tube for characterization. ^{1}H NMR (400 MHz, $CDCl_3$, ppm): δ 1.91 (s, 3H), 7.10-7.21 (m, 4H), 721-7.30 (m, 2H, overlapping with $CHCl_3$), 7.39-7.47 (m, 2H).

Synthesis of intermediate 5. To a fire dried three necked bottle was added 2,4-dibromo-3,5-dimethylthiophene (12.75 g, 47.23 mmol) and 220 mL dry THF. The mixture was cooled to 195 K and 2.4 mol L^{-1} *n*-BuLi (21.00 mL, 14.40 mmol) was introduced dropwise. After 1 h, trimethyl borate (7.0 mL, 61.64 mmol) was introduced. The resulting mixture was kept at 195 K for another 2 h. Then the mixture was warmed to room temperature and stayed overnight. 1-iodo-4-methoxybenzene (19.00 g, 76.28 mmol), $[Pd(PPh_3)_4]$ (0.70 g, 0.61 mmol), and aqueous Na_2CO_3 (100 mL, 2.5 mol L^{-1}) were added and the resulting mixture was allowed to reflux under Ar for 9 h. After cooling to room temperature, the mixture was poured into water, and extracted with dichloromethane. The organic layer was separated and dried with anhydrous Na_2SO_4. After concentration, the residual was purified by flash column chromatography (silica, petroleum ether) to obtain a crude product and then recrystallized from methanol to give **5** (11.31 g, 80.6%): white powders. ^{1}H NMR (400 MHz, $CDCl_3$, ppm): δ 2.22 (s, 3H), 2.41 (s, 3H), 3.82 (s, 3H), 6.93 (d, J = 8.6 Hz, 2H), 7.31 (d, J = 8.6 Hz, 2H). ^{13}C NMR (100 MHz, $CDCl_3$, ppm): δ 15.18, 15.50, 55.36, 113.52, 114.02, 126.98, 130.24, 131.72, 131.74, 134.46, 159.12. HRMS (ESI positive ion mode for $[M + H]^+$): Calcd for $C_{13}H_{14}OSBr$, 296.9949; found: 296.9946.

Synthesis of *o*-DAE 3 (mixer of 3a and 3p). *o*-DAE **3** (yellow powders, 0.85 g, 47.7%) was prepared by a similar procedure with DAE **1**, employing **5** (11.00 g, 37.01 mmol) and 4,5-dibromobenzo[1,2-*c*:3,4-*c'*]bis[1,2,5]thiadiazole (1.00 g, 2.84 mmol).

Separation of 3a and 3p. *o*-DAE **3** was slowly recrystallized from dichloromethane/methanol to give two types of crystals with different colours (yellow for **3a** and slight yellow for **3p**). Each kind of crystals was large enough for manual separation (purity around 94%), and the collected samples were recrystallized again from dichloromethane/methanol, separately, to give the conformers **3a** and **3p** with purity over 99%. **3a:** ^{1}H NMR (400 MHz, $CDCl_3$, ppm): δ 1.91 (s, 6H), 2.05 (s, 6H), 3.84 (s, 6H), 6.94 (d, J = 8.7 Hz, 4H), 7.37 (d, J = 8.6 Hz, 4H). ^{13}C NMR (100 MHz, $CDCl_3$, ppm): δ 14.73, 15.40, 55.35, 113.92, 127.21, 130.38, 132.15, 132.46, 133.32, 135.22, 136.00, 147.40, 157.28, 158.81. HRMS (ESI positive ion mode for $[M + H]^+$): Calcd for $C_{32}H_{27}N_4O_2S_4$, 627.1017; found: 627.1013. **3p:** ^{1}H NMR (400 MHz, $CDCl_3$, ppm): δ 1.84 (s, 6H), 2.12 (s, 6H), 3.84 (s, 6H), 6.94 (d, J = 8.6 Hz, 4H), 7.36 (d, J = 8.6 Hz, 4H). ^{13}C NMR (100 MHz, $CDCl_3$, ppm): δ 15.15, 15.22, 55.36, 113.93, 127.24, 130.35, 132.14, 132.33, 133.55, 135.17, 136.48, 147.39, 157.24, 158.80. HRMS (ESI positive ion mode for $[M + H]^+$): Calcd for $C_{32}H_{27}N_4O_2S_4$, 627.1017; found: 627.1018.

3 Results and discussion

Molecular design and synthesis. In order to acquire the steric effects in BBT-bridged DAEs, the choice of aryl groups with different steric sizes is of great importance. In practice, substituted benzofurans, benzothiophenes and thiophenes have been commonly employed as heteroaryl components for thermally irreversible DAEs. Therefore, adopting these aryl groups, we constructed four DAEs **1**-**4** with different steric sizes (Fig. 1a). DAEs **1** and **2** can be classified as one category with similar benzo-conjugated five-membered rings (benzofuran and benzothiophene), while DAEs **3** and **4** belong to the common dithienylethene series with slight difference in extra methyl groups.

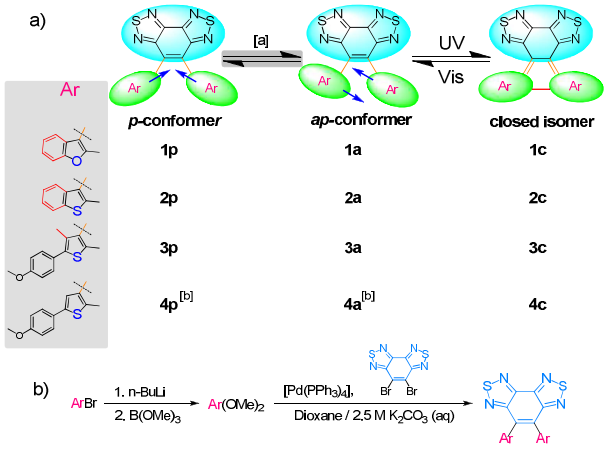

Fig. 1 a) Chemical structures of DAEs **1**-**4** with *p*- and *ap*-conformers and corresponding closed isomers. b) General synthetic routes to *o*-DAEs **1**-**4**. Note: [a] The exchanging rate between the *p*- and *ap*-conformers depends on the steric hindrance. [b] Coexisting conformer **4a** and **4p** are not separable, thus they are generally regarded as a pure compound **4o**.

The syntheses of *o*-DAEs **2** and **4** have previously been reported by our group.[43,45] General synthetic routes for the new *o*-DAEs **1** and **3** are summarized in Fig. 1b. Suzuki cross-coupling reactions of dibromo-BBT and corresponding arylboronates with the catalysis of $[Pd(PPh_3)_4]$ in a mixture of aqueous K_2CO_3 (2.5 M) and 1,4-dioxane gave the target *o*-DAEs **1** and **3**. The *ap*- and *p*-conformers of *o*-DAE **4** coexist in solution, whereas *o*-DAE **1** can be temporarily resolved into **1a** and **1p**, which are still slowly interconvertible in solution. Differently, the conformers of *o*-DAE **2** and **3** are sufficiently

stable to allow the separations. All the *c*-DAEs, except **3c**, could also be obtained owing to their excellent thermal stability. Their chemical structures were fully characterized by ^{1}H and ^{13}C NMR spectroscopy as well as high-resolution mass spectrum (HRMS); in the case of new compounds **1c**, **3a**, and **3p** the structures were further confirmed by X-ray crystallography (Table S4†).

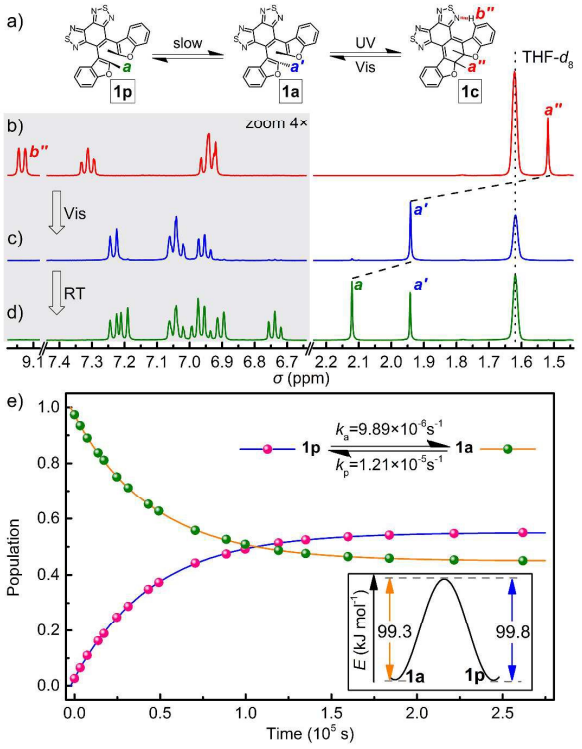

Fig. 2 a) Interconversion relationship of **1a**, **1p**, and **1c**. ^{1}H NMR spectroscopic changes of **DAE 1** in THF-d_8: b) **1c** and c) **1a** generated from **1c** by visible irradiation; d) equilibrium state of **1a** and **1p**. The low-field (marked with shadow) is magnified by 4 folds for better presentation. e) Time-dependent isomerism from **1a** to **1p** at 293 K. Inset in e): the experimental activation energies of **1a** and **1p**.

NMR spectroscopic analysis. To better present the isomerism and photochromism of DAE **1**, the ^{1}H NMR spectrum of its closed isomer **1c** was first investigated in THF-d_8. The spectrum of **1c** shows only one signal for the methyl protons (δ = 1.52 ppm, Fig. 2b), suggesting its C_2 symmetry. Meanwhile, at the low field, the characteristic double-peak for benzene protons H_b (δ = 9.14 ppm) indicates the possible existence of intramolecular hydrogen bonds between the H_b and N atoms. Upon visible light irradiation (λ > 470 nm), the peak of the methyl protons moved to lower field (δ = 1.94 ppm), which should be ascribed to the emergence of the *ap*-conformer **1a** (Fig. 2c). However, after **1c** being completely consumed, the spectrum started to evolve proportionately over time. Most notably, the partial signal of the methyl protons gradually shifted downfield to δ = 2.12 ppm, suggesting the formation of a new component. For most open isomers (*o*-DAEs), due to the deshielding effect from the facing aryls, the methyls in the *ap*-conformer are usually located at higher field[23,47] than those in the *p*-conformer. Thus, the new component could be confidently identified as the *p*-conformer **1p**. After standing for around 83 h at 293 K, an equilibrium state was eventually reached with a ratio of 45:55 (**1a**:**1p**; Fig. 2d). According to the time-dependent data, the isomerization rates between **1a** and **1p** were calculated as 1.21 × 10^{-5} s^{-1} and 9.89 × 10^{-6} s^{-1} (Fig. 2e), respectively, which are about 4-5 order of magnitude slower than those of common DAEs.[23,48] Based on the Eyring equation, the corresponding activation energies were determined to be 99.3 and 99.8 kJ mol^{-1}, respectively. Here, the *p*-conformer **1p** is slightly more stable, in contrast with those perfluorocyclopentene based DAEs, whose *ap*-conformer usually tends to take the dominant position.[20]

When the oxygen atom (benzofuran) in DAE **1** is replaced with sulfur atom (benzothiophene) in the next period, DAE **2** endows quite similar ^{1}H NMR spectra[45] as those in DAE **1**. It is noteworthy that the chemical shift of H_b in **2c** is much smaller (δ = 8.00 ppm), illustrating that the intramolecular hydrogen bond in **2c** is hampered to some extent. Therefore it can be inferred that in **2c** the benzene parts have worse planarity with the extended thiadiazoles, which is caused by their steric congestion. As for *o*-isomers, the congestion is also remarkable, therefore, **2a** and **2p** are totally stable and do not show any isomerism even after being kept at 343 K for 72 h. Thus, it can be concluded that changing the side aryls from benzofuran to benzothiophene increases the energy barrier between the *ap*- and *p*-conformers, and eventually eliminate their interconversion under ambient temperature.

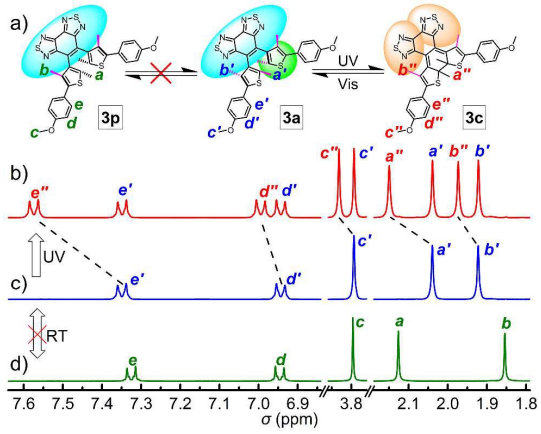

Fig. 3 a) Interconversion among **3a**, **3p**, and **3c**. ^{1}H NMR spectroscopic changes of DAE **3** in THF-d_8: b) **3a** upon UV irradiation at 302 ± 20 nm; c) pure *ap*-conformer **3a**; d) pure *p*-conformer **3p**.

Distinct ^{1}H NMR signals can be also found in the *ap*- and *p*-conformers of DAE **3** and **4** with similar dithienylethene structures. As for *o*-DAE **4**, the two conformers **4a** and **4p** give two independent signals, typically their α-methyl peaks locating at δ = 2.00 and 2.09 ppm, respectively. It is found that **4a** and **4p** always keep a fixed equilibrium ratio of 44:56 at 293 K, even during either photocyclization or cycloreversion (Fig. S1†). Apparently, *o*-DAE **4** behaves like ordinary DAEs, showing

fast conformation interconversions around the time-scale of ^{1}H NMR measurements. However, for *o*-DAE **3**, the conformers **3a** and **3p** were found to be separable, and showed well thermal stability at 343 K for 72 h (Fig. S2†), comparable to that of **2a** and **2p**. In the ^{1}H NMR spectra (Fig. 3c and 3d), the peaks of the *α*-methyl protons (H_a) for **3a** and **3p** appears at δ = 2.04 and 2.13 ppm, respectively, close to the chemical shifts of **4a** and **4p**. Interestingly, the signals of extra *β*-methyl protons (H_b) in **3a** and **3p** are both located at even higher field (δ = 1.92 for **3a**, 1.85 for **3p**, also see Fig. S15 and S19†), which can only be explained as the deshielding effect from the BBT bridge. Obviously, these extra *β*-methyls must be spatially sufficiently close to the thiadiazole units of the ethene bridge, testifying the steric congestion among those adjacent aryl groups. Upon UV irradiation (λ = 302±20 nm) to **3a**, all the peaks undergo notable upfield shifts, especially that of H_a (δ = 2.15 ppm), indicating the formation of the *c*-isomer **3c** (Fig. 3b). The distinct behavior of DAEs **3** and **4** clearly shows that the introduction of *β*-methyls onto thiophene rings can also sufficiently block the interconversion between the *ap*- and *p*-conformers.

Molecular structure analysis. In order to gain further insight into the steric effects on both *o*- and *c*-DAEs, X-ray crystallography and quantum chemical calculations on ground-state conformations were performed. The geometries of the DAEs were optimized by density functional theory (DFT) calculations. Unless otherwise noted, the hybrid B3LYP functional[49,50] and the triple-zeta 6-311G(d,p) basis set were employed in the calculations,[51] with solvent effects taken into account by the polarizable continuum model (PCM)[52] and dispersion corrections included by the D3 version of Grimme's dispersion with Becke-Johnson damping,[53] respectively, as implemented in the Gaussian 09 program package.[54]

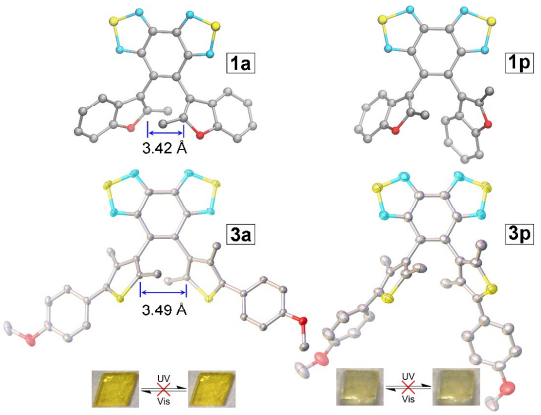

Fig. 4 Optimized ground-state geometries (up) of **1a** and **1p**, and ORTEP representation (bottom) of crystal structures in **3a** and **3p** with displacement ellipsoids shown at the 50% probability level. For clarity, hydrogen atoms were not shown. Inset images show the crystals of **3a** and **3p** upon photo-irradiation.

Compared with *o*-DAE **2**, it is difficult to obtain the single crystals of *o*-DAE **1** suitable for X-ray diffraction (XRD), which may be due to the slow isomerism between *ap*- and *p*-conformers. Instead, favourable geometries of **1a** and **1p** were calculated from the optimized structures of *o*-DAE **1**. The distance between the reactive carbons in **1a** is 3.42 Å, being slightly smaller than that in **2a** (3.49 Å from crystal data and 3.47 Å from DFT calculations),[45] ensuring the appropriate distance for the photocyclization. As shown in Fig. 4, the oxygen atoms of benzofuran in **1a** are smaller than the sulfur atoms of benzothiophene ring in **2a**, and thus the space between benzene parts and BBT bridge can be a little larger. This subtle structural difference releases the congestion between the bridge and aryls, and thus makes the slow flip of aryls become possible in *o*-DAE **1**.

For DAE **3**, its *ap*- and *p*-conformers (**3a** and **3p**) are found to be spontaneously resolved into two kinds of bulky crystals during the slow recrystallization in CH_2Cl_2/MeOH (Fig. 4). In fact, we have successfully utilized this phenomenon to separate these two conformers (See Experimental section). According to crystal analyses, **3a** endows a slightly more coplanar structure than **3p**, which should be responsible for its deeper colour. Moreover, the structure of **3p** shows no significant difference from that of similar derivative DAE **4o**, which crystallizes into the *p*-conformer (**4p**).[44] Owing to spatial crowdedness the extra *β*-methyls in *o*-DAE **3** are expected to collide with the BBT plane during rotational motion of the thiophene rings. In this way, rotation of the thienyl group is restricted to a small range by the steric effects, which enables the thermal separation of *ap*- and *p*-conformers. Therefore, the *β*-methyls in *o*-DAE **3** work in a similar way to the conjugated benzenes of the benzothiophenes in *o*-DAE **2**, which can be further supported by the non-photochromism in the single crystal state. In general, a photochromic single crystal of *o*-DAEs should meet two basic requirements: i) crystallization into the *ap*-conformer, and ii) sufficiently short distance between the two reactive carbon atoms, typically less than 4.2 Å.[55-57] The crystals of the *ap*-conformers **2a** and **3a** both appeared to be photo-inert, despite their favorable distance in the range of 3.49 Å between the reactive carbon atoms (Fig. 4). Along with our previous work,[45] the violation of the empirical rules can be attributed to the excess intramolecular hindrance accompanied with the restricted packing stress in the lattice, which eventually suppresses the photochromism in the crystal state.

The closed isomers covalently fix the two aryls and the BBT ethene bridge to form a nearly coplanar structure; their geometries are therefore very useful to evaluate the structurally steric congestions. Fig. 5 shows the ORTEP drawings of **1c** and analogue **2c** based on crystallographic analyses. It can be seen that the distances between the aryl H atoms and the N atoms in the ethene bridge are much shorter than the sum of their van der Waals radii (2.60 Å), indicating the existence of intramolecular hydrogen bonds. The bond lengths in **1c** (2.25 Å and 2.25 Å) are shorter than those in **2c** (2.26 and 2.46 Å), suggesting a stronger binding in the former. Moreover, in these *c*-isomers, the planar BBT bridge exhibits a distorted conformation around the photochromic cyclohexadiene center, where the torsion angle is expected to reflect the steric effects. The comparison between the torsion angels of **1c** (12.3°) and **2c** (31.3°) suggest that the steric

hindrance in **1c** is considerably smaller, in agreement with the results in the ring-open state.

Unfortunately, we failed to obtain the single crystals of **3c** and **4c**, and thus we employed the optimized ground-state conformation to further illustrate the steric effects. As seen from Fig. 5, a large torsion angle between cyclohexadiene and the BBT bridge (33.2°) can be also found in **3c**, while **4c** adopts an almost coplanar geometry (6.1°). Apparently, the two *β*-methyls play an important role to hamper the planarity, almost to the same extent as the benzenes in **2c**. Compared with those in **4c**, the anisoles in **3c** also show considerable torsion to the cyclohexadiene unit. Such two kind of torsions appear to have great influence on the optical properties, especially the absorption wavelength, which will be demonstrated below.

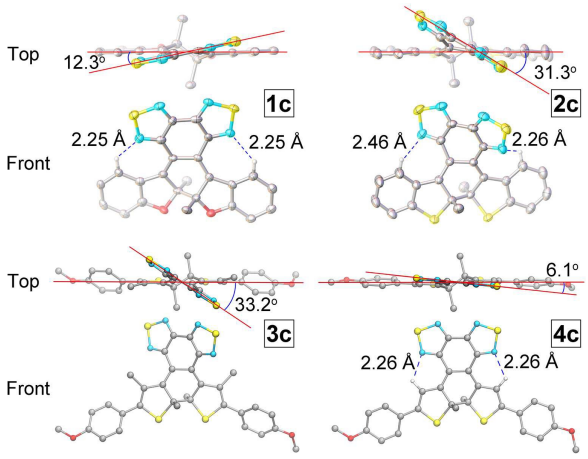

Fig. 5 Optimized ground-state geometries (bottom) of **3c** and **4c**, and ORTEP representation (up) of the crystal structures of **1c** and **2c**[45] with displacement ellipsoids shown at the 50% probability level. For clarity, hydrogen atoms were not shown.

For more detailed information on the steric effects, we employed DFT calculations at the B3LYP/6-31G(d,p) level of theory to illustrate the rotation energy of single bond connecting aryl groups to BBT bridge in *o*-DAE **1**-**4** (Fig. 6). The results suggest an order of the energy barriers as **2o** > **3o** > **1o** > **4o**. Like common DAEs, the rotational barrier of **4o** is located at 72 kJ mol^{-1}, and its *ap*- and *p*-conformers can thus quickly exchange to each other in the solution. However, the barrier of **3o** with extra small *β*-methyls on the thiophenes increases sharply up to over 135 kJ mol^{-1}, which is almost twice as large as that of **4o**. Furthermore, benzene-conjugated thiophenes in **2o** can even boost the barrier to the highest one[45] (> 140 kJ mol^{-1}). Such large barriers in **2o** and **3o** can completely turn off the interconversion between the two conformers at room temperature (half-life time over 10^3 year). As a comparison, the similar benzofuran derivative **1o** gives a much lower barrier of 99 kJ mol^{-1}, which indicates a significantly shorter half-life time of around a dozen of hours, which agrees well with the experimental data. Clearly, in BBT-based DAEs, introducing any substituents (rather than small protons) at the *β*-position of thiophenes would increase the rotational barrier and slow down the interconversion between the *ap*- and *p*-conformers, which benefits the isolation of the photo-active *ap*-conformers.

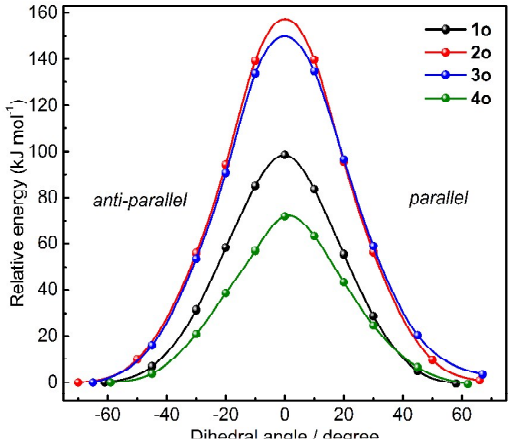

Fig. 6 Calculated relative energies of conformers in *o*-DAEs **1**-**4** with respect to dihedral angle between the BBT bridge and side aryls. The negative dihedral angle corresponds to the *ap*-conformer, while the positive dihedral angle corresponds to the *p*-conformer.

We further optimized the parallel ↔ anti-parallel transition states for the ring-open isomers of four photochromic compounds, as shown in Fig. S4. At the transition states, the BBT bridging unit is significantly bent owing to strong steric hindrance in the molecules. The bent angles are much more significant in **2o** and **3o**, rendering their high energy barriers for the parallel ↔ anti-parallel interconversion. The bent angle of BBT is smaller in **1o**, and becomes even smaller than 10° in **4o**. We in addition examined the non-planarity of the aryl rings and the BBT bridges. For the aryl ring, which is either furan or thiophene ring colliding with the BBT bridge, we selected the six heavy atoms from the aromatic ring and the *α*-methyl group, and fitted a plane through their Cartesian coordinates. The root-mean-square-distance (RMSD, in Å) from these points to the fitted plane was then calculated as the indicator of the "non-planarity", as shown in Table S2. Clearly, the aryl ring in **2o** and **3o** show greater non-planarity, with RMSD larger than 0.1 Å. The RMSD in the other two compounds are consistently smaller. The non-planarity of the BBT bridging unit was also calculated using all its twelve heavy atoms. Again, only those for **2o** and **3o** exceed 0.2 Å. The order **2o** ≈ **3o** > **1o** > **4o** is consistent with the bent angles shown in Fig. S4, and also in accordance with the estimated energy barriers.

Optical properties and photochromism. When dissolved in tetrahydrofuran (THF), all *o*-DAEs **1**-**4** appear almost colourless with few absorption bands in the visible range. As shown in Fig. 7, their absorption spectra (pure *ap*-conformer of *o*-DAEs **1**-**3** and unresolved conformers of *o*-DAE **4**) show intense absorption in the range of 270-350 nm and moderate absorption between 350 and 450 nm. Upon UV irradiation at 313 nm, the transparent solution of *o*-DAEs **1**-**4** turned orange, reddish orange, purplish red, and dark green, respectively.

New broad absorption peaks emerged at around 517, 522, 569, and 654 nm, indicating the formation of the corresponding ring-closed isomers **1c**-**4c** (Fig. 7). It should be noticed that the absorption maxima of previously reported benzothiophene-based *c*-DAEs are commonly much longer than that of benzofuran derivatives in the visible region.[58] However, **2c** exhibits a red-shift of only 5 nm (0.02 eV) compared with **1c**, and the two *c*-isomers endow a very similar absorption pattern. We believe that the distorted feature of **2c** slightly hampers the conjugation of the photochromic cyclohexadiene, and thus shortening its absorption maximum. A more significant phenomenon can also be found in **3c** and **4c**, whose structural difference refers just to the methyls pointing to the BBT bridge. Compared with **4c**, **3c** shows a dramatic hypsochromic shift, as large as 85 nm (0.28 eV), of absorption maximum, and loses almost all the fine structure in the absorption spectrum as well.

o-DAEs **1**-**4** exhibit moderate fluorescence (Fig. 7 and Table 1) originating from intramolecular charge transfer (ICT) from the donor (aryls) to the acceptor (BBT). Owing to the different electron-donating ability of benzofurans and benzothiophenes, **2a** shows yellowish-green emission (λ_{max} = 492 nm), which is in slightly longer wavelength than the bright cyan light emitted by **1a** (λ_{max} = 514 nm). Differently, the orange fluorescence from **3a** (λ_{em} = 600 nm) and **4o** (the unseparable mixture of **4a** and **4p**, λ_{em} = 584 nm) are much weaker, which might be ascribed to the excess vibrational relaxation pathways that deactivate the excited state. No significant fluorescence signals could be observed in the corresponding *c*-DAEs, except that **3c** exhibits an unusual weak NIR emission (fluorescence quantum yield, φ_F = 0.2%), which may arise from the overcrowded feature. During the photocyclization process, the fluorescence emissions of *o*-DAEs were gradually quenched, in consistency with the conversion ratios (Table 1) at the photostationary state (PSS). Clearly, the quenching mainly arises from the loss in the fluorescent *o*-DAE.

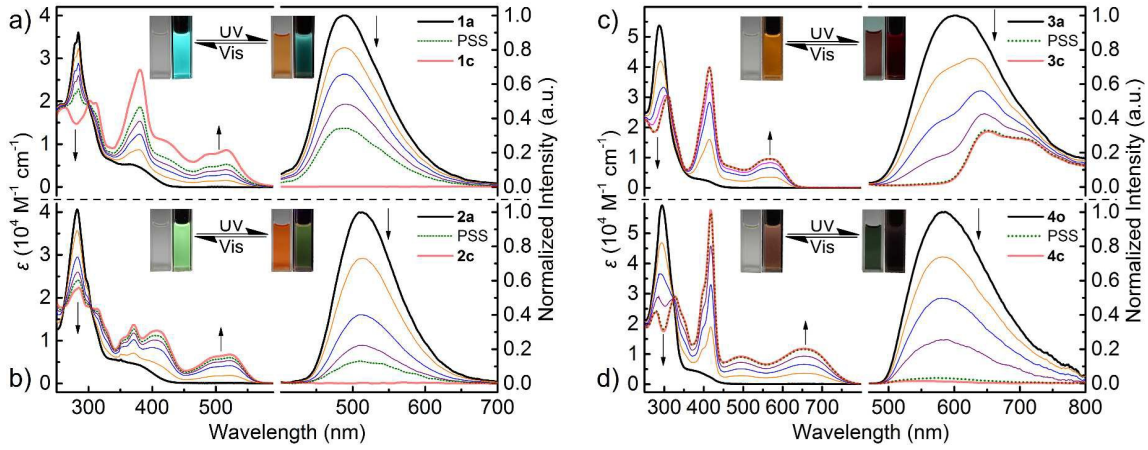

Fig. 7 Absorption and fluorescence changes of a) **1a**, b) **2a**, c) **3a**, and d) **4o** in THF upon UV irradiation at 313 nm, along with those of the corresponding ring-closed isomers. Excitation for fluorescence is set at each isobestic point. Inset images show the colour and emission changes triggered by UV (λ = 313 nm) and visible (λ > 470 nm) light. Note: **1a** in a) was *in situ* generated from **1c** by visible irradiation within 1 min. The absorbance and fluorescence of **3c** in c) is calculated from the spectra.

Table 1 Spectroscopic Data of DAEs **1**-**4** in THF

DAE	λ_{max} [nm][a] (ε [10^3 M^{-1} cm^{-1}])	λ_{em} [nm][a]	Φ_F [%][b]	$\Phi_{o\text{-}c}$ [%][c]	$\Phi_{c\text{-}o}$ [%][c]	*CR* [%][d]
1a	284 (36.1)	488	0.56	55	—	62
1c	517 (8.6)	—	—	—	12.4	>99
2a	282 (40.6)	514	3.36	73	—	90
2c	522 (6.8)	—	—	—	8.6	>99
3a	288 (53.7)	600	0.78	68	—	>99
3c	569 (9.5)	651	—	—	9.0	>99
4o	295 (59.2)	584	0.30	32	—	>99
4c	654 (11.8)	—	—	—	1.1	>99

[a]Typical absorption (λ_{max}) and emission maxima (λ_{em}) of *o*-DAE in UV region and *c*-DAE in the visible region, respectively. [b]Fluorescence quantum yield (Φ_F). [c]Quantum yields of photocyclization ($\Phi_{o\text{-}c}$) at 313 nm and cycloreversion ($\Phi_{c\text{-}o}$) at 517 nm. [d]Conversion ratio from *o*- to *c*-isomer (irradiation at λ = 313 nm) or from *c*- to *o*-isomer (irradiation at λ > 470 nm).

For common *o*-DAEs, since the photo-active *ap*-conformer usually possesses about half of the population, the photocyclization quantum yield ($\Phi_{o\text{-}c}$) in solution is usually limited within 50%. *o*-DAE **4o** is a typical example whose $\Phi_{o\text{-}c}$ at 313 nm is 32%, since the ratio of its *ap*-conformer **4a** is only 45%. As for the pure *ap*-conformers **1a**, **2a**, and **3a**, their $\Phi_{o\text{-}c}$ are measured as 55%, 73%, and 68%, respectively, which are considerably higher than the commonly observed $\Phi_{o\text{-}c}$. The deviation from the theoretic value (100%) should be mainly explained as the excess steric effects[59] along with the deleterious ICT progress, which may open some competing deactivating channels in excited states.[24,45] On another hand, the cycloreversion quantum yields of **1c**, **2c** and **3c** ($\Phi_{c\text{-}o}$~10%) are found to be much higher than that of **4c** (1.1%), which is expected to correlate more with their sterically congested features than the differences in the heteroaryls. Based on the above, introducing steric hindrance into BBT-based DAEs would eventually increase both $\Phi_{o\text{-}c}$ and $\Phi_{c\text{-}o}$.

Thermal stability of ring-closed isomers. Previously, we found that employing the low aromatic BBT as the ethene bridge is beneficial for building up a thermally irreversible photochromic DAE system (typically, DAE **4**).[43,44] However, as presented above, this extended bridge also imposes a great steric hindrance on the linked heteroaryl groups in both ring-open and ring-closed states, which is commonly thought to disrupt the thermal stability of the *c*-isomers. Thus, it is necessary to check the thermal stability of **1c**, **2c**, and **3c** with the pronounced hindrance, in comparison with the regular DAE **4c**. Indeed, **3c** turned out to be less stable than the others even when it was kept at ambient temperature, and its coloured solution faded away following first-order reaction kinetics (Fig. 8a). Moreover, the fading rates are found to increase with the solvent polarity (1.46×10^{-5}, 2.49×10^{-5}, and 3.13×10^{-5} s^{-1} in toluene, THF, and acetonitrile, respectively). However, even in the polar acetonitrile solvent, **1c** and **2c** exhibit no apparent thermal back-reactions at 333 K after 800 min (Fig. S5†), similarly to **4c** with much less steric hindrance. Obviously, there must be some specific reasons accounting for the unusual thermal stability of **1c** and **2c**.

To this end, DFT calculations were performed on the ground energy difference ($|\Delta E_{ap\text{-}c}|$) between the ring-open (*anti*-parallel) and ring-closed isomers.[60,61] As shown in Table 2, the energy difference follows the order DAE **4** < **1** < **2** ≈ **3**, indicating that the *c*-isomer **3c** indeed is the least stable with respect to the corresponding *o*-isomer **3a**, consistent with its experimental thermal bleaching. Moreover, considering all DAEs **1**-**4** endowing heteroaryl groups with low aromatic stabilization energy, the differentiation in $|\Delta E_{ap\text{-}c}|$ should mainly result from the steric hindrance in the *c*-isomers. For example, **2c** and **3c** possess similar large steric hindrances, and thus show the highest value. However, it is apparent that the large ground state energy difference in DAE **2** cannot explain its considerable thermal stability in the coloured *c*-isomer.

Consequently, more detailed calculations were conducted to follow the thermal ring-opening process, particularly the activation energy. As can be seen from Fig. 8b and Table 2, **1c** and **4c** endow similar high activation energies over 120 kJ mol^{-1} in THF, while the energy decrease to 114.6 kJ mol^{-1} for **2c** and then 95.6 kJ mol^{-1} for **3c**. Here, the very low activation energy in **3c** approves its thermally fading feature, and the much higher values in the rest *c*-DAEs confirm their considerable thermal stability. To better understand these differences, hydrogen bonds between the BBT bridge (N) and the aryl rings (H) were examined. During the ring-opening process, the hydrogen bond length is enlarged, thus costing extra energy to reach the transition state. Noteworthy, the changes of the N-H bond distance from the *c*-isomers to the transition states indeed follow the order DAE **2** < **4**

< **1**, which agrees well with the activation energy. As for **3c**, which lacks the hydrogen bonds, the energy barrier is rather low and results in its rapid thermal fading. Moreover, the energies of the ring-closed state, transition state and ring-open state in DAE **3** are found to shift with the solvents. Its transition state (**3-TS**) is more sensitive to the solvent effects than the *c*-isomer (Fig. S6†), leading to a slightly increased reaction barrier (96.7 kJ mol^{-1}) in toluene and a decreased barrier (94.8 kJ mol^{-1}) in acetonitrile, in consistence with the experimental results. Therefore, the intramolecular hydrogen bond in the BBT bridged DAEs can effectively increase the ring-open activation energy, compensate the steric hindrance effects, and finally stabilize the coloured *c*-isomers.

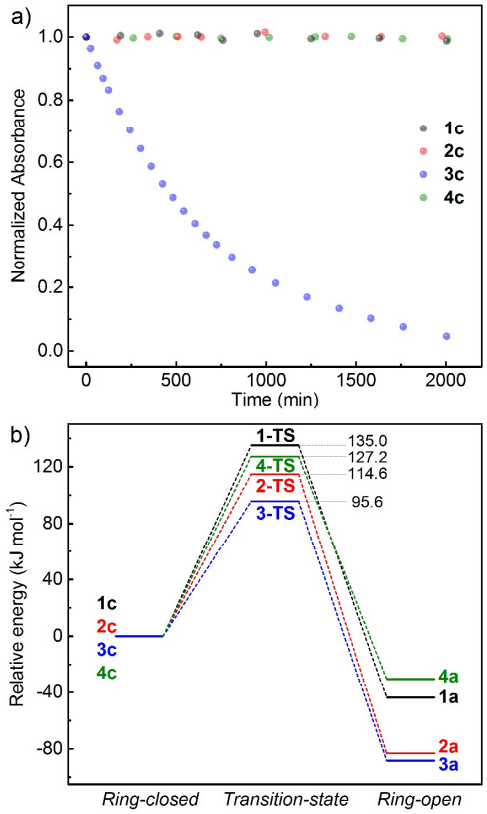

Fig. 8 a) Decay curves of **1c**-**4c** in THF at 293 K. b) Computed barrier of the thermal ring-opening processes of **1c**-**4c** in THF.

Table 2 Computed ground and transition state energies, and hydrogen bond (N-H) length of DAEs **1**-**4** in THF.

DAE	N-H Bond Length [Å]			Energy [kJ mol^{-1}]	
	L_c[a]	L_{TS}[a]	$\Delta L_{TS\text{-}c}$	$\Delta E_{ap\text{-}c}$[b]	$\Delta E_{TS\text{-}c}$[c]
1	2.20	2.48	0.28	-43.7	135.0
2	2.33	2.46	0.13	-83.1	114.6
3[d]	—	—	—	-88.4	95.6
4	2.26	2.51	0.25	-30.2	127.2

[a]Hydrogen bond length of *c*-isomer at the ground state (L_c) and the transition state (L_{TS}). [b]Ground energy difference between *ap*- and *c*-isomers. [c]Energy difference between ground and transition states of *c*-isomers. [d]No hydrogen bond in **3c**.

4 Conclusions

We have systematically investigated the steric effects on the photochromic DAEs **1**-**4** with the BBT bridge. In the ring-open state, the isomerization between *ap*- and *p*-conformers is governed by the rotation barrier (DAE **4** < **1** < **3** ≈ **2**) generated by the intramolecular steric hindrance from the BBT bridge and adjacent aryls. Specifically, **4a** and **4p** are in fast interconversion, and **1a** slowly converts to **1p**, while **2a** and **3a** become thermally stable at ambient temperature. The separated *ap*-conformers (**1a**-**3a**) show high photo-sensitivity with $\Phi_{o\text{-}c}$ over the conventional limitation of 50% in common DAEs. In the ring-closed state, the steric effects are also prominent, as suggested by the torsions between the photochromic cyclohexadiene and the ethene bridge (**4c** < **1c** < **2c** ≈ **3c**), and accordingly, disrupt the thermal stability of the *c*-isomers. However, the intramolecular hydrogen bonds in **1c**, **2c**, and **4c** enlarge the ring-opening activation barriers, and thus effectively stabilize the *c*-isomers. Considering both switching performance and thermal irreversibility, DAE **2** is the most balanced structure serving as a novel building block for highly photo-sensitive photochromic system. This work provides insight into the steric effects on the isomerism and photochromism of DAEs, along with a unique approach to develop high efficient photochromic materials.

Acknowledgements

This work was supported by National 973 Program (No. 2013CB733700), NSFC for Creative Research Groups (21421004) and Distinguished Young Scholars (21325625), NSFC/China, the Oriental Scholarship, Science and Technology Commission of Shanghai Municipality (15XD1501400), and the Fundamental Research Funds for the Central Universities (WJ1416005). Xin Li and Hans Ågren acknowledge the Swedish National Infrastructure for Computing (SNIC) for providing computational resources.

Notes and references

1 M. Irie, T. Fukaminato, T. Sasaki, N. Tamai and T. Kawai, *Nature*, 2002, **420**, 759.
2 H. Tian and Y. Feng, *J. Mater. Chem.*, 2008, **18**, 1617.
3 S. J. Chen, L.-J. Chen, H.-B. Yang, H. Tian and W. H. Zhu, *J. Am. Chem. Soc.*, 2012, **134**, 13596.
4 B. M. Neilson and C. W. Bielawski, *J. Am. Chem. Soc.*, 2012, **134**, 12693.
5 M. Bälter, S. Li, J. R. Nilsson, J. Andréasson and U. Pischel, *J. Am. Chem. Soc.*, 2013, **135**, 10230.
6 W. A. Velema, J. P. van der Berg, M. J. Hansen, W. Szymanski, A. J. M. Driessen and B. L. Feringa, *Nat. Chem.*, 2013, **5**, 924.
7 G. Lv, B. Cui, H. Lan, Y. Wen, A. Sun and T. Yi, *Chem. Commun.*, 2015, **51**, 125.
8 S. Iamsaard, S. J. Asshoff, B. Matt, T. Kudernac, J. J. L. M. Cornelissen, S. P. Fletcher and N. Katsonis, *Nat. Chem.*, 2014, **6**, 229.
9 Y. Wu, Y. S. Xie, Q. Zhang, H. Tian, W. H. Zhu and A. D. Q. Li, *Angew. Chem. Int. Ed.*, 2014, **53**, 2090.
10 K.-Y. Chen, O. Ivashenko, G. T. Carroll, J. Robertus, J. C. M. Kistemaker, G. London, W. R. Browne, P. Rudolf and B. L. Feringa, *J. Am. Chem. Soc.*, 2014, **136**, 3219.
11 K. Higashiguchi, G. Taira, J.-i. Kitai, T. Hirose and K. Matsuda, *J. Am. Chem. Soc.*, 2015, **137**, 2722.
12 V. Aubert, V. Guerchais, E. Ishow, K. Hoang-Thi, I. Ledoux, K. Nakatani and H. Le Bozec, *Angew. Chem. Int. Ed.*, 2008, **47**, 577.
13 A. M. Asadirad, S. Boutault, Z. Erno and N. R. Branda, *J. Am. Chem. Soc.*, 2014, **136**, 3024.
14 F. Luo, C. B. Fan, M. B. Luo, X. L. Wu, Y. Zhu, S. Z. Pu, W. Y. Xu and G. C. Guo, *Angew. Chem. Int. Ed.*, 2014, **53**, 9298.
15 M. Berberich, A.-M. Krause, M. Orlandi, F. Scandola and F. Würthner, *Angew. Chem. Int. Ed.*, 2008, **47**, 6616.
16 G. Jiang, Y. Song, X. Guo, D. Zhang and D. Zhu, *Adv. Mater.*, 2008, **20**, 2888.
17 T. Fukaminato, T. Doi, N. Tamaoki, K. Okuno, Y. Ishibashi, H. Miyasaka and M. Irie, *J. Am. Chem. Soc.*, 2011, **133**, 4984.
18 S.-J. Lim, J. Seo and S. Y. Park, *J. Am. Chem. Soc.*, 2006, **128**, 14542.
19 R. C. Shallcross, P. Zacharias, A. Köhnen, P. O. Körner, E. Maibach and K. Meerholz, *Adv. Mater.*, 2013, **25**, 469.
20 M. Irie, T. Fukaminato, K. Matsuda and S. Kobatake, *Chem. Rev.*, 2014, **114**, 12174.
21 K. Higashiguchi, K. Matsuda, N. Tanifuji and M. Irie, *J. Am. Chem. Soc.*, 2005, **127**, 8922.
22 M. Herder, B. M. Schmidt, L. Grubert, M. Pätzel, J. Schwarz and S. Hecht, *J. Am. Chem. Soc.*, 2015, **137**, 2738.
23 K. Uchida, Y. Nakayama and M. Irie, *Bull. Chem. Soc. Jpn.*, 1990, **63**, 1311.
24 M. Irie and K. Sayo, *J. Phys. Chem.*, 1992, **96**, 7671.
25 J. J. D. de Jong, L. N. Lucas, R. Hania, A. Pugzlys, R. M. Kellogg, B. L. Feringa, K. Duppen and J. H. van Esch, *Eur. J. Org. Chem.*, 2003, 1887.
26 R. Gostl, B. Kobin, L. Grubert, M. Patzel and S. Hecht, *Chem. Eur. J.*, 2012, **18**, 14282.
27 M. Hanazawa, R. Sumiya, Y. Horikawa and M. Irie, *J. Chem. Soc., Chem. Commun.*, 1992, 206.
28 Y. Chen, D. X. Zeng and M. G. Fan, *Org. Lett.*, 2003, **5**, 1435.
29 K. Suzuki, T. Ubukata and Y. Yokoyama, *Chem. Commun.*, 2012, **48**, 765.
30 J. C.-H. Chan, W. H. Lam and V. W.-W. Yam, *J. Am. Chem. Soc.*, 2014, **136**, 16994.
31 T. Nakashima, M. Goto, S. Kawai and T. Kawai, *J. Am. Chem. Soc.*, 2008, **130**, 14570.
32 V. Lemieux, M. D. Spantulescu, K. K. Baldridge and N. R. Branda, *Angew. Chem. Int. Ed.*, 2008, **47**, 5034.
33 H. Tian, B. Chen, H. Y. Tu and K. Müllen, *Adv. Mater.*, 2002, **14**, 918.
34 S.-C. Pang, H. Hyun, S. Lee, D. Jang, M. J. Lee, S. H. Kang and K.-H. Ahn, *Chem. Commun.*, 2012, **48**, 3745.
35 H. Ogawa, K. Takagi, T. Ubukata, A. Okamoto, N. Yonezawa, S. Delbaere and Y. Yokoyama, *Chem. Commun.*, 2012, **48**, 11838.

36 K. Morinaka, T. Ubukata and Y. Yokoyama, *Org. Lett.*, 2009, **11**, 3890.
37 S. Fukumoto, T. Nakashima and T. Kawai, *Angew. Chem. Int. Ed.*, 2011, **50**, 1565.
38 T. Nakashima, R. Fujii and T. Kawai, *Chem. Eur. J.*, 2011, **17**, 10951.
39 M. Takeshita and T. Yamato, *Angew. Chem. Int. Ed.*, 2002, **41**, 2156.
40 H. Jin-nouchi and M. Takeshita, *Chem. Eur. J.*, 2012, **18**, 9638.
41 S. Aloïse, M. Sliwa, Z. Pawlowska, J. Réhault, J. Dubois, O. Poizat, G. Buntinx, A. Perrier, F. Maurel, S. Yamaguchi and M. Takeshita, *J. Am. Chem. Soc.*, 2010, **132**, 7379.
42 M. Walko and B. L. Feringa, *Chem. Commun.*, 2007, 1745.
43 W.H. Zhu, Y. H. Yang, R. Metivier, Q. Zhang, R. Guillot, Y. S. Xie, H. Tian and K. Nakatani, *Angew. Chem. Int. Ed.*, 2011, **50**, 10986.
44 Y. H. Yang, Y. S. Xie, Q. Zhang, K. Nakatani, H. Tian and W. H. Zhu, *Chem. Eur. J.*, 2012, **18**, 11685.
45 W. L. Li, C. H. Jiao, X. Li, Y. S. Xie, K. Nakatani, H. Tian and W. H. Zhu, *Angew. Chem. Int. Ed.*, 2014, **53**, 4603.
46 W. L. Li, X. Li, Y. S. Xie, Y. Wu, M. Q. Li, X.-Y. Wu, W.-H. Zhu and H. Tian, *Sci. Rep.*, 2015, **5**, 9186.
47 M. Irie and M. Mohri, *J. Org. Chem.*, 1988, **53**, 803.
48 M. Takeshita and M. Irie, *J. Org. Chem.*, 1998, **63**, 6643.
49 A. D. Becke, *J. Chem. Phys.*, 1993, **98**, 5648.
50 C. Lee, W. Yang and R. Parr, *Phys. Rev. B*, 1988, **37**, 785.
51 R. Krishnan, J. S. Binkley, R. Seeger and J. A. Pople, *J. Chem. Phys.*, 1980, **72**, 650.
52 J. Tomasi, B. Mennucci and R. Cammi, *Chem. Rev.*, 2005, **105**, 2999.
53 S. Grimme, S. Ehrlich and L. Goerigk, *J. Comput. Chem.*, 2011, **32**, 1456.
54 M. J. Frisch, G. W. Trucks, H. B. Schlegel, G. E. Scuseria, M. A. Robb, J. R. Cheeseman, G. Scalmani, V. Barone, B. Mennucci, G. A. Petersson, H. Nakatsuji, M. Caricato, X. Li, H. P. Hratchian, A. F. Izmaylov, J. Bloino, G. Zheng, J. L. Sonnenberg, M. Hada, M. Ehara, K. Toyota, R. Fukuda, J. Hasegawa, M. Ishida, T. Nakajima, Y. Honda, O. Kitao, H. Nakai, T. Vreven, J. A. Montgomery Jr., J. E. Peralta, F. Ogliaro, M. J. Bearpark, J. Heyd, E. N. Brothers, K. N. Kudin, V. N. Staroverov, R. Kobayashi, J. Normand, K. Raghavachari, A. P. Rendell, J. C. Burant, S. S. Iyengar, J. Tomasi, M. Cossi, N. Rega, N. J. Millam, M. Klene, J. E. Knox, J. B. Cross, V. Bakken, C. Adamo, J. Jaramillo, R. Gomperts, R. E. Stratmann, O. Yazyev, A. J. Austin, R. Cammi, C. Pomelli, J. W. Ochterski, R. L. Martin, K. Morokuma, V. G. Zakrzewski, G. A. Voth, P. Salvador, J. J. Dannenberg, S. Dapprich, A. D. Daniels, Ö. Farkas, J. B. Foresman, J. V. Ortiz, J. Cioslowski and D. J. Fox, Gaussian, Inc., Wallingford, CT, USA, 2009.
55 S. Kobatake, K. Uchida, E. Tsuchida and M. Irie, *Chem. Commun.*, 2002, 2804.
56 K. Shibata, K. Muto, S. Kobatake and M. Irie, *J. Phys. Chem. A*, 2002, **106**, 209.
57 M. Morimoto and M. Irie, *Chem. Commun.*, 2005, 3895.
58 T. Yamaguchi and M. Irie, *J. Org. Chem.*, 2005, **70**, 10323.
59 T. Yamaguchi and M. Irie, *J. Photochem. Photobiol. A*, 2006, **178**, 162.
60 P. D. Patel and A. E. Masunov, *J. Phys. Chem. C*, 2011, **115**, 10292.
P. D. Patel, I. A. Mikhailov, K. D. Belfield and A. E. Masunov, *Int. J. Quantum Chem.*, 2009, **109**, 3711.

Sterically hindered diarylethenes with a benzobis(thiadiazole) bridge: photochemical and kinetic studies†

Wenlong Li, Yunsong Cai, Xin Li, Hans Ågren He Tian and Wei-Hong Zhu**

Based on the benzobis(thiadiazole)-bridged diarylethenes, the exchanging rate between the main conformers in the ring-open form gradually slows down, offering the opportunity to isolate the photoactive *anti*-parallel conformer. In the ring-closed state, the excess steric hindrance can disrupt the thermal bistability.